

Coupling of quasi-localized and phonon modes in glasses at lowfrequency

Jun Duan(段军), Song-Lin Cai(蔡松林), Gan Ding(丁淦), Lan-Hong Dai(戴兰宏), and Min-Qiang Jiang(蒋敏强)

Citation: Chin. Phys. B, 2024, 33 (**5**): 056502. DOI: 10.1088/1674-1056/ad2dce
Journal homepage: http://cpb.iphy.ac.cn; http://iopscience.iop.org/cpb

What follows is a list of articles you may be interested in

Rolling structure from bilayer nanofilm by mismatch

Jian-Gang Li(李建刚), Xiao-Pi Geng(耿小丕), Qian-Nan Gao(高倩男), Jun Zhu(朱俊), Zhi-Xiang Gao(高志翔), and Hong-Wei Zhu(朱弘伟)

Chin. Phys. B, 2023, 32 (**12**): 126201. DOI: 10.1088/1674-1056/ace032

Electronic structure of YbB_6 dependent on onsite Coulomb interaction *U* and internal parameter of B atom

Hong-Bin Wang(王宏斌), Li Zhang(张莉), Jie Duan(段婕)

Chin. Phys. B, 2019, 28 (**11**): 116201. DOI: 10.1088/1674-1056/ab46a1

Thermal conductivity of systems with a gap in the phonon spectrum

E Salamatov

Chin. Phys. B, 2018, 27 (**7**): 076502. DOI: 10.1088/1674-1056/27/7/076502

Thermal effect on endurance performance of 3-dimensional RRAM crossbar array

Nianduan Lu(卢年端), Pengxiao Sun(孙鹏霄), Ling Li(李泠), Qi Liu(刘琦), Shibing Long(龙世兵), Hangbing Lv(吕杭炳), Ming Liu(刘明)

Chin. Phys. B, 2016, 25 (**5**): 056501. DOI: 10.1088/1674-1056/25/5/056501

Enhancing the thermal conductivity of polymer-assisted deposited Al_2O_3 film by nitrogen doping

Huang Jiang (黄江), Zhang Yin (张胤), Pan Tai-Song (潘泰松), Zeng Bo (曾波), Hu Guo-Hua (胡国华), Lin Yuan (林媛)

Chin. Phys. B, 2012, 21 (**12**): 126501. DOI: 10.1088/1674-1056/21/12/126501

Coupling of quasi-localized and phonon modes in glasses at low frequency

Jun Duan(段军)[1,2], Song-Lin Cai(蔡松林)[1,2], Gan Ding(丁淦)[1], Lan-Hong Dai(戴兰宏)[1,2], and Min-Qiang Jiang(蒋敏强)[1,2,†]

[1] *State Key Laboratory of Nonlinear Mechanics, Institute of Mechanics, Chinese Academy of Sciences, Beijing* 100190, *China*
[2] *School of Engineering Science, University of Chinese Academy of Sciences, Beijing* 101408, *China*

(Received 25 January 2024; revised manuscript received 25 February 2024; accepted manuscript online 28 February 2024)

Boson peak of glasses, a THz vibrational excess compared to Debye squared-frequency law, remains mysterious in condensed-matter physics and material science. It appears in many different kinds of glassy matters and is also argued to exist in damped crystals. A consensus is that boson peak originates from the coupling of the (quasi)-localized non-phonon modes and the plane-wave-like phonon modes, but the coupling behavior is still not fully understood. In this paper, by modulating the content of localized modes and the frequencies of phonon modes, the coupling is clearly reflected in the localization and anharmonicity of low-frequency vibrational modes. The coupling enhances with increasing cooling rate and sample size. For finite sample size, phonon modes do not fully intrude into the low frequency to form a dense spectrum and they are not sufficiently coupled to the localized modes, thus there is no Debye level and boson peak is ill-defined. This suggestion remains valid in the presence of thermal motions induced by temperature, even though the anharmonicity comes into play. Our results point to the coupling of quasi-localized and phonon modes and its relation to the boson peak.

Keywords: metallic glasses, low-frequency vibrational modes, plane wave, boson peak

PACS: 65.60.+a, 62.20.D–, 62.25.Jk **DOI:** 10.1088/1674-1056/ad2dce

1. Introduction

Unlike their ordered counterparts, long-range disordered glasses exhibit anomalous thermal and transport properties at low temperatures.[1–3] One of the most intriguing phenomena is the significantly enhanced low-temperature heat capacity, which is mainly ascribed to the abnormal acoustic excitation at the frequency of THz.[1] This excess low-frequency vibration, which is shown as an obvious peak in the plot of Debye-reduced vibrational density of states $g(\omega)/\omega^2$, has been widely observed in various glasses with different scales and interactions, such as metallic glasses,[4,5] network glasses,[6] polymeric glasses,[7] colloidal glasses,[8] disordered granular packings,[9] and even damped crystals.[10] The peak, termed as boson peak (BP), attracts considerable interests in condensed-matter physics and material science. In the past decades, many viewpoints have been put forward to explain the emergence of BP, including phonon–saddle transition,[11] temporal fluctuations of atomic environment,[12] heterogeneous elasticity induced by disorder,[13] Ioffe–Regel limit of transverse phonons,[14] hierarchical potential energy landscape with marginal stability,[15] smeared out van Hove singularity,[16] and, more recently, quasi-localized vibration of string-like dynamical defects.[17] Besides, great efforts have been devoted to construct structural and dynamical parameters to reveal the microscopic origin of BP. These parameters contain local inversion symmetry,[18] orientational order,[19] vibrational mean-squared displacements,[20] flexibility volume,[21] and so on.

Despite much controversy in various viewpoints, it is generally accepted that BP originates from the coupling of localized non-phonon modes and transverse phonon modes, which causes a complete reconstruction of vibrational density of states (VDOS) at low frequencies.[14,22,23] A localized mode centers at a disordered core with length scale approaching ten atoms, and decays away from it in the form of $\sim r^{-2}$, where r denotes the distance from the core.[24] These disordered cores are loosely packed[25] and highly distorted.[26] The patterns of localized modes are very similar to that of Eshelby-like shear transformations,[27] i.e., elementary rearrangement events in glasses. Indeed, these cores have strong tendency to undergo irreversible rearrangement under the stimuli of thermal activation[28] or mechanical loading.[29–32] Thus, the disordered cores of localized modes are considered as the unstable structural defects or "soft spots".[29] On the other hand, phonon modes arise from the translational symmetry of system's Hamiltonian. In a finite-size system, their frequencies are quantized into a discrete set of bands, which are broaden by the intrinsic disorder of glasses.[33]

Soft spots with much lower shear resistance, distributing randomly in the elastic matrix, destroy the homogeneous elasticity of glasses in nanoscale, which is the basic assumption of Debye theory. The heterogeneous elasticity in space results in the significant scattering[14] and damping[34] of transverse phonons. Thus, elastic wave is inhibited to propagate and

†Corresponding author. E-mail: mqjiang@imech.ac.cn

© 2024 Chinese Physical Society and IOP Publishing Ltd

continually attenuates in the propagation process, which is reflected by the resonant coupling of non-propagating localized modes and propagating phonon modes form the perspective of atomic vibration. Such competition of propagation and attenuation leads to the emergence of BP, which is supported by the consistence of the frequency of BP and the Ioffe–Regel limit of transverse phonons.[14] The transverse characteristic of BP is also evidenced by Yang *et al.*[19] They found that BP correlates near perfectly with a pure structural parameter, named as orientational order to represent the easiest shear direction of an atom, both in space and statistics.

The significant coupling of localized modes and phonon modes at low frequencies is indicated by the spatially-hybridized patterns of the vibrational modes: many localized cores superpose on the plane-wave-like background. Recently, Lerner and Bouchbinder[35] clearly observed these hybridized patterns and produced an original method to successfully extract the localized contribution from the highly-hybridized BP modes. By separating atomic vibrations into phonon subspace and non-phonon subspace, Caroli and Lemaitre[23] found that the coupling between phonon subspace and non-phonon subspace is necessary to account for the property of acoustic propagation and attenuation. But for finite sample size, phonon modes and localized modes at low frequencies may not couple sufficiently to each other, indicated by the well-identified localized modes by participation ratio[36] and the discrete set of phonon bands.[33] This insufficient coupling may influence the boson peak at higher frequency. Therefore, the coupling behavior is still not fully understood and deserves further investigation. In this paper, using molecular dynamics simulations, we modulate the coupling effects by varying the content of localized modes with cooling rates and the frequencies of phonon modes with sample sizes. The coupling intensity between low-frequency vibrational modes and the shape of VDOS are carefully investigated.

2. Simulation methods

Due to their structural simplicity, similar to the random densepacking of spheres, metallic glasses are an ideal model system for a large variety of glassy matters. Finnis–Sinclair type embedded atom method potential[37] is adopted to simulate $Cu_{50}Zr_{50}$ metallic glasses using molecular dynamics software LAMMPS. Periodic boundary conditions are applied on all three dimensions. The temperature and pressure are controlled with Nosé–Hoover thermostat and Parrinello–Rahman barostat, respectively. The external pressure maintains at zero during the sample preparation process. Firstly, a cubic sample consisting of 10976 atoms is thermally equilibrated at 2000 K for 2 ns that is much longer than its structural relaxation time. Then, the equilibrated liquid is continuously cooled to 0 K with cooling rates ranging from 10^{10} K/s to 10^{13} K/s; see Fig. 1(a) for the cooling history. After being cooled to 0 K, the sample is additionally in-depth relaxed to a local potential energy minimum by conjugate gradient algorithm with fixed simulation box. Now, we obtain a zero-temperature glass sample. Besides, an instantaneously quenched sample is prepared by minimizing potential energy of the equilibrated liquid right after 2-ns high-temperature relaxation. To modulate phonon modes, we also prepare samples cooled at 10^{12} K/s with various atom numbers, ranging from 2048 to 10976. Ten independent samples in each preparation condition are prepared to reduce statistical fluctuation.

By diagonalizing dynamical matrix of the system, we obtain the frequencies ω and polarization vectors $\boldsymbol{\Psi}$ of harmonic vibrational modes.[31] The VDOS is obtained by the statistics of frequencies

$$g(\omega) = \frac{1}{3N-3}\sum_j \frac{1}{\sqrt{\pi}\sigma}\exp\left(-\frac{(\omega-\omega_j)^2}{\sigma^2}\right), \tag{1}$$

where N is the number of atoms and σ is the smooth parameter of Gaussian function. σ is set to 0.2 to obtain a smooth and precise VDOS. Denominator $3N-3$ denotes the total number of vibrational modes except three translational modes. Participation ratio[38] is adopted to measure the localized degree of each vibrational mode, which is defined as

$$\mathrm{PR} = \frac{\left(\sum_i |\psi_i|^2\right)^2}{N\sum_i |\psi_i|^4}, \tag{2}$$

where ψ_i is the projection of polarization vectors ψ on atom i. Participation ratio ranges from $1/N$ (fully localized) to 1 (fully extended) and equals $2/3$ for a plane-wave mode. A parameter, similar to the Grüneisen parameter[39] but not normalized by the vibrational frequency, is used to measure the anharmonicity of a vibrational mode

$$\chi = \frac{\Delta\omega}{\varepsilon_\mathrm{v}}. \tag{3}$$

This parameter denotes the frequency variation $\Delta\omega$ of a vibrational mode under volume deformation. A vanishing value means a very small anharmonicity. To compute this parameter, a slight dilation with volumetric strain $\varepsilon_\mathrm{v} = 10^{-8}$ is applied on the zero-temperature sample and then the potential energy is minimized. The evolution of each vibrational mode is carefully discriminated, based on the concept of "identifiable mode", the same mode at different strain configurations, proposed by us.[31]

For a three-dimensional system, Debye level is related to the density of atom number n, transverse velocity of sound c_T, and longitudinal velocity of sound c_L, that is

$$A_\mathrm{D} = \left(c_\mathrm{L}^{-3} + 2c_\mathrm{T}^{-3}\right)/(6\pi^2 n). \tag{4}$$

Transverse and longitudinal velocities of sound can be calculated by $c_\mathrm{T} = \sqrt{G/\rho}$ and $c_\mathrm{L} = \sqrt{(B+4G/3)/\rho}$, respectively.

G is the athermal shear modulus, B is the athermal bulk modulus, and ρ is the density of mass. To compute athermal elastic moduli, a slight deformation with strain $\varepsilon = 10^{-8}$ (along direction in each of xx, yy, zz, xy, xz, yz) is applied on the zero-temperature sample and then the potential energy is minimized. The moduli are obtained by the linear elastic fit of stress–strain responses.

Another widely used method to obtain VDOS utilizes velocity auto-correlation function (VACF) of the system in NVT ensemble.[40] To proceed, the zero-temperature sample is heated to a given temperature, ranging from 0.1 K to 500 K (well below the glass transition temperature), by assigning appropriate velocity to each atom. A thermal relaxation at the given temperature for 1 ns is performed to stabilize the sample. Then, the position $\boldsymbol{x}$ and velocity $\boldsymbol{v}$ of each atom are recorded in the following relaxation process to calculate mean-squared displacements (MSD) and VACF of the system. The MSD is

$$\mathrm{MSD}(t) = \left\langle \left(\boldsymbol{x}_i(t_0+t) - \boldsymbol{x}_i(t_0)\right)^2 \right\rangle_{i,t_0}, \tag{5}$$

and the VACF is

$$\mathrm{VACF}(t) = \langle \boldsymbol{v}_i(t_0)\cdot\boldsymbol{v}_i(t_0+t)\rangle_{i,t_0} / \langle \boldsymbol{v}_i(t_0)\cdot\boldsymbol{v}_i(t_0)\rangle_{i,t_0}, \tag{6}$$

where angular bracket denotes the average over atom i, the initial time t_0, and ten independent samples. Taking Fourier transform of VACF, we get VDOS of the system.

3. Results and discussion

Figure 1(b) shows the radial distribution function (RDF) of samples with different cooling rates. The disordered structure of samples is confirmed by the rapid decay of the fluctuation of curves. The split of second peaks is a typical feature of $Cu_{50}Zr_{50}$ metallic glasses.[41] As the cooling rate increases, the samples become more disordered, which is indicated by the less sharp peaks on the RDF; see inset in Fig. 1(b) for clarity. During the glass formation process, structural frustration inhibits crystallization and retains some of the structural characteristics of the glass-forming liquid.[42] The higher cooling rate results in less structural relaxation time, driving the supercooled liquid to deviate from internal equilibrium and enter the glassy state earlier; see the increasing glass transition temperature in Fig. 1(a). Therefore, the glass samples with higher cooling rates inherit more free volume and structural disorder from the glass-forming liquid, and have more high-energy structural defects. These unstable structural defects bring about soft localized vibrations, i.e., low-frequency quasi-localized modes. Thus, the samples with higher cooling rates possess more localized modes, which is consistent with the discovery that more rejuvenated samples with higher energy have more low-frequency localized modes.[36,43]

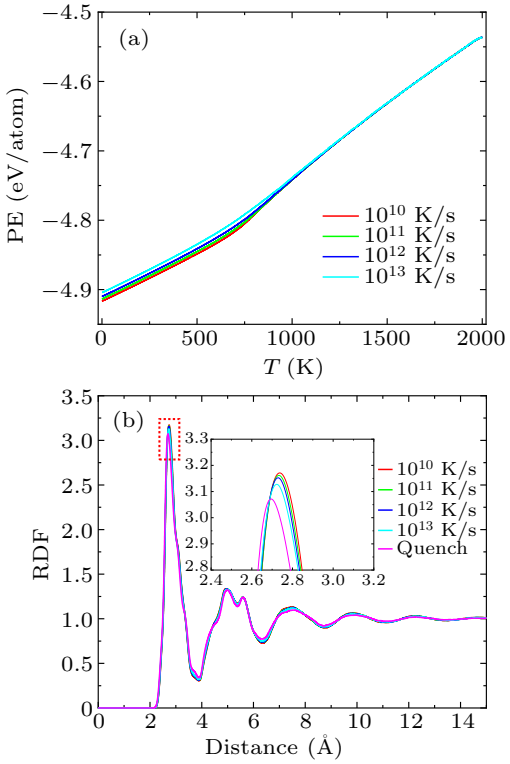


Fig. 1. (a) The cooling history dependence of potential energy on temperature for samples with 10976 atoms and different cooling rates. The deflection of a curve indicates the glass transition process and the corresponding temperature increases with increasing cooling rate, giving rise to more rejuvenated samples. (b) The radial distribution function for samples with 10976 atoms and different cooling rates. Inset is the magnification of region enclosed by red dashed window.

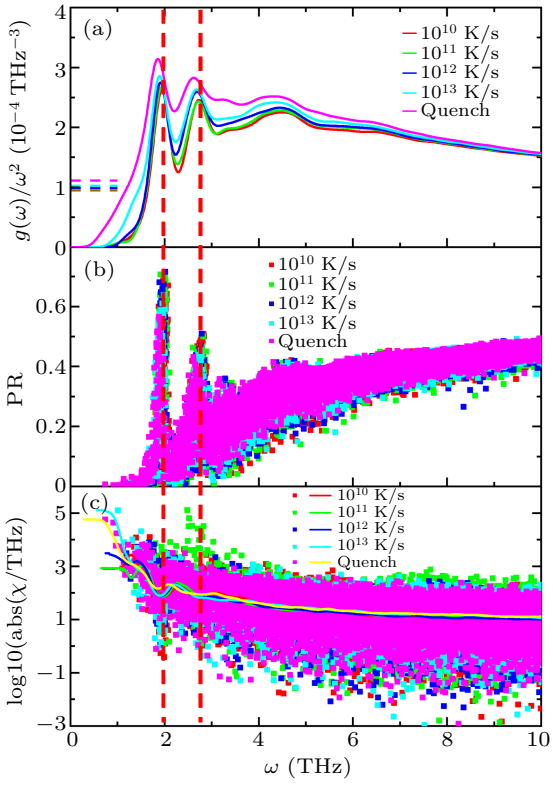


Fig. 2. (a) Reduced VDOS, (b) participation ratio, and (c) anharmonicity parameter for samples with 10976 atoms and different cooling rates. The horizontal dashed lines at zero frequency in panel (a) denote Debye level calculated by samples' elasticity. The curves in panel (c) are obtained by coarse-graining the scattered points with Gaussian function. The red vertical dashed lines represent the frequencies of the first and second phonon bands.

Figure 2(a) shows the reduced VDOS of samples with different cooling rates. For samples of finite size, the phonon modes appear as discrete frequency bands. The first and second bands, corresponding respectively to transverse phonons at the frequencies of $2\pi c_{\mathrm{T}}/L$ and $2\sqrt{2}\pi c_{\mathrm{T}}/L$ (L is the linear size of system), are clearly shown as peaks in Fig. 2(a). As suggested by Bouchbinder and Lerner,[33] phonon bands are broadened by disorder in glasses with peaks' width depending on the strength of disorder σ, phonon frequency ω, degeneracy level n_{b} (number of phonon modes at the band), and atom number N, i.e., $\sim \sigma\omega\sqrt{n_{\mathrm{b}}}/\sqrt{N}$. Consistent with this suggestion, phonon bands become broader with increasing cooling rates and the second bands are much broader than the first ones. For higher frequencies, the significant damping causes phonon modes to stop propagating and become diffusive, making the phonon bands blur and eventually disappear.[14,44,45] The elastic softening caused by increasing cooling rates leads to the uplift of Debye level calculated by samples' elasticity; the data are given in Table 1. However, finite sample size results in the first phonon band occurring at frequency $\omega_{\mathrm{T}} = 2\pi c_{\mathrm{T}}/L$ much higher than zero, leading to the reduced VDOS displays a gap near zero frequency and not reach the calculated Debye level. Thus, there is no Debye level in the reduced VDOS. Even though, a significant excess of low-frequency vibration over Debye level around 3 THz is observed.

Table 1. Shear modulus G, bulk modulus B, transverse velocity of sound c_{T}, longitudinal velocity of sound c_{L}, Debye level A_{D}, and the lowest frequency of transverse phonon ω_{T} for samples with 10976 atoms and different cooling rates.

Cooling rate (K/s)	10^{10}	10^{11}	10^{12}	10^{13}	Quench
G (GPa)	25.493	25.239	24.796	24.248	22.881
B (GPa)	107.863	107.839	107.448	106.931	105.307
c_{T} (m/s)	1858.366	1849.465	1833.660	1813.940	1763.797
c_{L} (m/s)	4383.730	4379.027	4365.041	4347.242	4297.318
A_{D} (10^{-4} THz^{-3})	0.951	0.965	0.990	1.023	1.113
ω_{T} (THz)	2.027	2.017	2.000	1.978	1.922

As shown by the participation ratio plot in Fig. 2(b), localized non-phonon modes and extended phonon modes coexist at low frequencies. Due to the proximity and overlap of their frequencies, strong resonant coupling between localized modes and phonon modes occurs, resulting in localized modes becoming more extend and phonon modes becoming more localized. The resonant coupling agrees with the finding that no localized modes survive within phonon bands.[33] The coupling behavior is demonstrated in the patterns of vibrational modes in Fig. 3. The localized mode in Fig. 3(a) has vibrational frequency $\omega = 1.563$ THz and participation ratio PR $= 0.00831$. Its polarization vectors localize at a disordered core and feature the Eshelby-like quadrupolar symmetry. The phonon mode with frequency $\omega = 1.871$ THz in Fig. 3(c) lies in the first phonon band. Its participation ratio PR $= 0.599$ is very close to the value of a plane-wave mode $(2/3)$, indicating that this phonon mode is spatially extended and has an obvious plane-wave characteristic. Clearly, there is no sign of localization and vortex-like elastic fields are observed. The vortex fields are found in many disordered solids and carry the elastic interactions between shear transformation events.[46] The frequency of the hybridized mode in Fig. 3(b), that is $\omega = 1.761$ THz, lies between the localized mode in Fig. 3(a) and the phonon mode in Fig. 3(c). The coupling effect allows this mode to combine the characteristics of the localized mode and the phonon mode: a much weaker localization at the disordered core superposing on a wave-like background with an intermediate participation ratio PR $= 0.0819$. Hybridized modes, widely present at low frequencies, reflect the elastic disturbance and interactions of soft spots and have been demonstrated to be highly correlated with the onset of plastic events[30] and the morphology of avalanche events.[31] Note that the case shown in Fig. 3 is simple but representative. Due to the strong coupling among many low-frequency vibrational modes, a large number of hybridized modes are very complex with many disordered cores, as observed by Lerner and Bouchbinder.[35]

The mechanism of resonant coupling indicates that localized modes couple to phonon modes of similar frequencies.[33] As the cooling rate increases, more localized modes are inherited from the liquid, indicated by the elevation of the low-frequency VDOS in Fig. 2(a). The resulting denser modes lead to stronger coupling between them, which is evidenced by the decrease in the difference of participation ratio between localized modes and phonon modes in Fig. 2(b).

The coupling effect is also reflected in the anharmonicity of the vibrational modes. As can be seen from Fig. 2(c), the lower the frequency the greater the anharmonicity of the modes, in agreement with the results of Xu *et al.*[39] Atomic displacements along the localized mode can reach sufficiently large values for which anharmonic effects in the interactive potential are appreciable.[47] Thus, for vibrational modes, stronger localization usually means stronger anharmonicity. Compared to the localized modes, phonon modes are considered to be less anharmonic. Whereas, the strong coupling makes the difference between them obscure. Only by coarse-

graining the scattered points with Gaussian function, can we see small valleys corresponding to the first phonon bands. The coarse-grain method is performed by

$$\log 10\left(\mathrm{abs}\left(\chi\left(\omega\right)\right)\right)=\frac{\sum\limits_{j}h\left(\omega-\omega_{j}\right)\log 10\left(\mathrm{abs}\left(\chi_{j}\right)\right)}{\sum\limits_{j}h\left(\omega-\omega_{j}\right)},\quad(7)$$

where $h(\omega)=1/\sqrt{\pi}\sigma\exp\left(-\omega^{2}/\sigma^{2}\right)$ is the Gaussian function with coarse-grain parameter $\sigma=0.1$. The valley becomes shallower with increasing cooling rates due to the enhanced coupling effect.

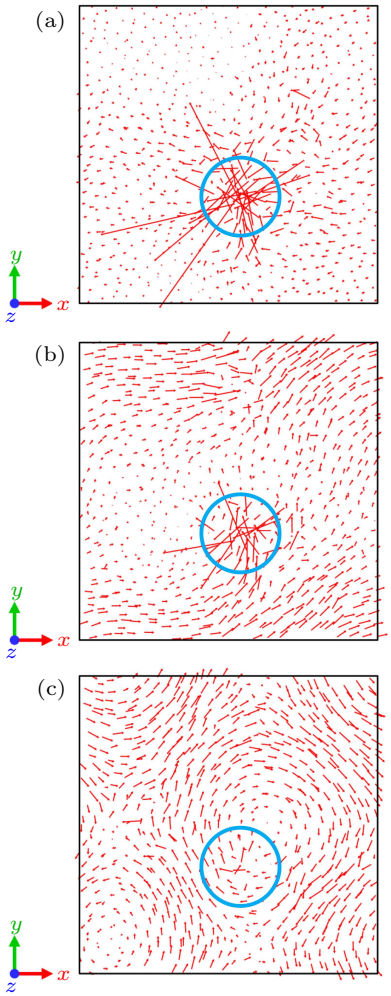


Fig. 3. The two-dimensional (2D) projective quiver plots of three representative coupled vibrational modes for a 10^{10}-K/s sample sliced at position $z=25$ Å with thickness $\delta z=4$ Å. (a) A localized mode with vibrational frequency $\omega=1.563$ THz and participation ratio PR = 0.00831. (b) A hybridized mode with $\omega=1.761$ THz and PR = 0.0819. (c) A phonon mode with $\omega=1.871$ THz and PR = 0.599. The blue circle denotes the disordered core of the localized mode.

We modulate the phonon modes by varying the system sizes. As the system size increases, phonons can appear at lower frequencies and the corresponding frequency bands shift to the left, as shown in Fig. 4. Note that the obtained phonon bands in Fig. 4 have frequencies slightly lower than the calculated phonon bands in Table 2, resulting from the reduction of frequencies caused by coupling effects as suggested in some theories.[22,23] Figure 4(a) displays that the calculated Debye level remains unchanged; see the data given in Table 2. A gap replacing the Debye level occurs near zero frequency in the reduced VDOS and becomes shorter with increasing sample size. Note that the second phonon band of sample size $N=10976$ shares the same frequency with the first phonon band of sample size $N=4000$. The degeneracy level of the second band ($n_{\mathrm{b}}=24$) is larger than that of the first band ($n_{\mathrm{b}}=12$). Compared to the first band of sample size $N=4000$, more phonon modes in the second band of sample size $N=10976$ lead to stronger coupling effects, which is evidenced by the smaller difference of participation ratio between localized modes and phonon modes in Fig. 4(b). With the increase of sample size, phonon modes intrude into lower frequency and become denser, resulting in stronger coupling effects between vibrational modes.

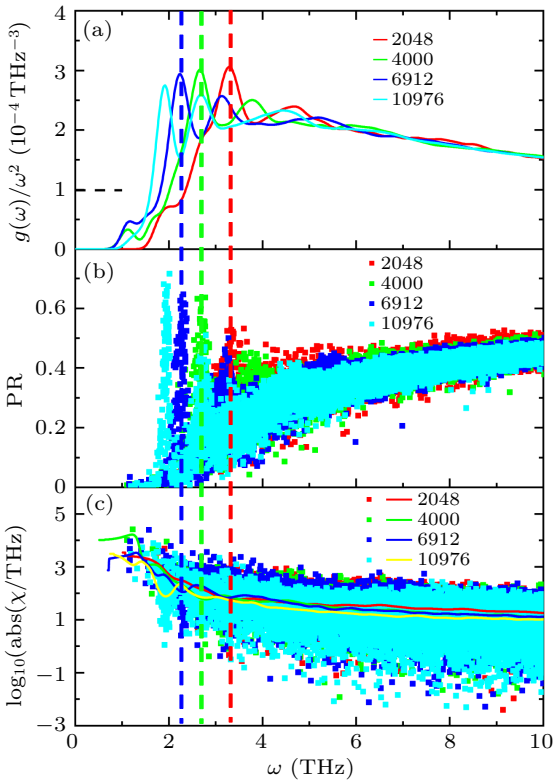


Fig. 4. (a) Reduced VDOS, (b) participation ratio, and (c) anharmonicity parameter for samples with 10^{12}-K/s cooling rate and different sample sizes. The horizontal dashed line at zero frequency in panel (a) denotes Debye level calculated by samples' elasticity. The curves in panel (c) are obtained by coarse-graining the scattered points with Gaussian function. The vertical dashed lines represent the frequencies of the first phonon bands, shifting to the left with increasing sample size.

At finite sample size, the absence of Debye level implies that BP, the breakdown of Debye prediction, is ill-defined. This claim is confirmed by the excess of low-frequency VDOS consisting of multiple peaks corresponding to discrete phonon bands that depend on the sample size. It is recognized that BP has a characteristic lengthscale of the order of a few interatomic distance, comparable to the spatial extent of the heterogeneous elasticity.[48,49] However, BP is still ill-defined when

sample size is larger than the BP length, e.g., the samples studied in this paper. We attribute it to the insufficient coupling between localized modes and phonon modes, indicated by the obvious difference of their participation ratio. Some theories argue that the coupling of localized modes and phonon modes causes a complete reconstruction of the VDOS and gives birth to the BP.[22,23] By projecting atomic vibrations into phonon subspace (corresponding to the plane-wave like phonons with large wavelength) and non-phonon subspaces (corresponding to the localized non-affine effects with small wavelength), Caroli and Lemaitre[23] found that the coupling between phonon subspace and non-phonon subspace is necessary for correctly capturing acoustic behavior in glasses. BP length as a natural lengthscale separates phonon subspace and non-phonon subspace. For finite sample size, discrete phonons modes are finite (few for small sample size) and the phonon subspace constructed by these phonons is incomplete, which leads to the insufficient coupling between phonon subspace and non-phonon subspace and the rugged VDOS with multiple phonon bands. As the thermodynamic limit is approached, phonon modes intrude into the low frequency to form a dense spectrum, the enhancement of coupling causes the localized modes to dissolve with the phonon modes.[33,47] The reduced VDOS reaches the calculated Debye level near zero frequency, and the rugged multiple peaks corresponding to phonon bands merge into a smooth peak, i.e., boson peak. Thus, the Debye level and BP are well-defined in the thermodynamic limit, in agreement with the experimental results.[50,51]

The vibrational modes obtained by diagonalizing the dynamical matrix contain only the topological information at the minimum of potential energy. For finite temperature, the system no longer resides at the minimum and is able to explore the surrounding region with the help of thermal motion. The vibrational modes obtained by VACF method reflect the real vibrations at the current temperature and contain topological information of the region that the system explores. Figure 5 shows the vibrational information at temperatures ranging from 0.1 K to 500 K below the glass transition temperature. The existence of plateau in the plot of temperature-reduced MSD in Fig. 5(a) indicates that the atoms in system are in a state of vibrations. The uplift of plateau with temperature indicates that the anharmonicity drives the atomic vibrations to deviate from the low-temperature harmonicity.

Table 2. Shear modulus G, bulk modulus B, transverse velocity of sound c_{T}, longitudinal velocity of sound c_{L}, Debye level A_{D}, and the lowest frequency of transverse phonon ω_{T} for samples with 10^{12}-K/s cooling rate and different sample sizes.

Atom number	2048	400	6912	10976
G (GPa)	24.807	24.775	24.786	24.796
B (GPa)	107.500	107.355	107.198	107.448
c_{T} (m/s)	1834.159	1832.681	1833.056	1833.660
c_{L} (m/s)	4366.403	4362.872	4360.451	4365.041
A_{D} (10^{-4} THz^{-3})	0.990	0.992	0.991	0.990
ω_{T} (THz)	3.500	2.798	2.332	2.000

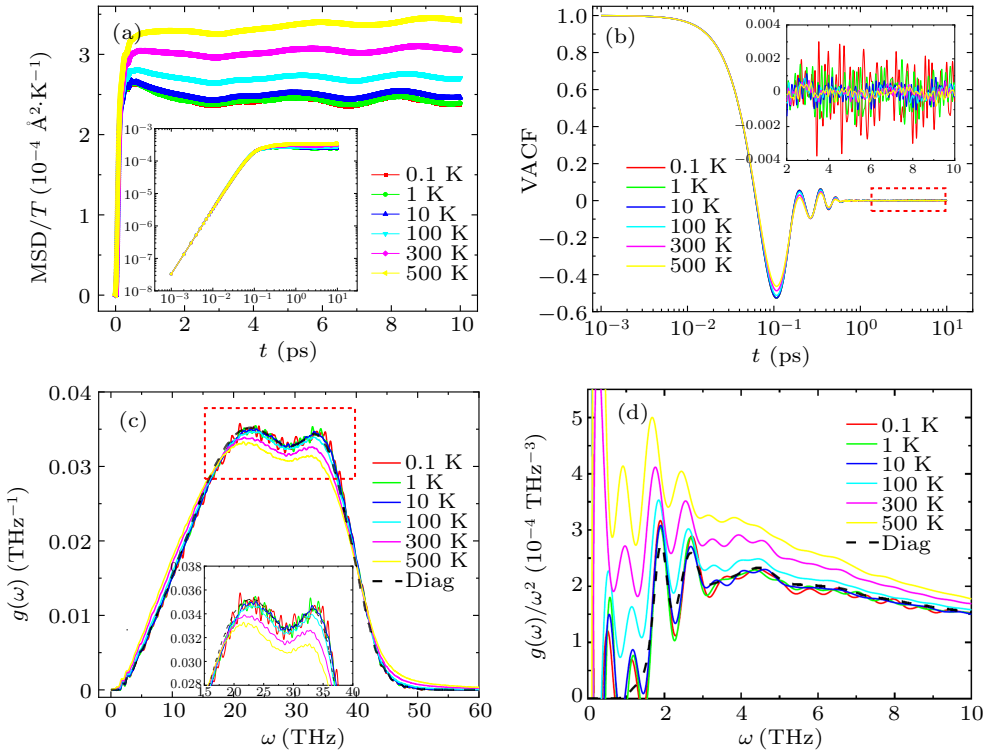


Fig. 5. (a) Temperature-reduced MSD, (b) VACF, (c) VDOS, and (d) reduced VDOS for samples with 10976 atoms and cooling rates 10^{12} K/s at different temperatures. Inset in panel (a) is the main plot in log–log scale. Insets in panels (b) and (c) are the magnification of regions enclosed by the red dashed window in the main plot. The dashed line in panel (d) represents the reduced VDOS obtained by diagonalizing (Diag) dynamical matrix of zero-temperature samples.

In order to fully explore the low-frequency vibrations, the integration time for the VACF needs to be long enough to be much larger than the vibrational period of the first phonon bands, e.g., $T = 2\pi/\omega_{\mathrm{T}} \approx 3.14$ ps for samples with 10976 atoms and cooling rate 10^{12} K/s. The integration time for all calculation is set to be 10 ps. As shown in Fig. 5(b), although the VACF has attenuated to a vanishing value after 1 ps, the long-term fluctuations containing low-frequency vibration information still exist. Note that the VACF is averaged on 100 initial time t_0 and 10 independent samples, so the long-term fluctuations are not due to the insufficient statistics. VDOS in Fig. 5(c) shows an obvious fluctuating structure, which appears across the entire frequency range and is particularly pronounced in the middle-frequency region. The fluctuating structure even gives rise to the anti-physical appearance that the reduced VDOS is negative at low frequency, clearly shown in Fig. 5(d). As the temperature approaches zero, the fluctuating structure in Fig. 5(c) becomes more pronounced, corresponding to the more significant long-term fluctuations of VACF in Fig. 5(b). This phenomenon may be related to the fractal free energy landscape at low temperatures,[52,53] where the system is not purely vibrational and undergoes weak relaxation.[54]

At low temperatures below 10 K, the curves in Fig. 5 collapse and the VDOS converges to its zero-temperature counterpart obtained by the diagonalization method. This is due to the negligible anharmonic effect caused by thermal motion, where the explored region is near the minimum of potential energy and its real topology can be represented by the topology of the minimum. As the temperature rises, the explored region expands and anharmonic effect comes into play. Temperature-induced sample softening causes an increase of the low-frequency vibration,[55] as shown in Figs. 5(c) and 5(d).

In the present work, the vibrational anharmonicity caused by thermal motion is not the focus of our attention. We choose 1 K as the calculated temperature of the VDOS obtained by the VACF method. Figures 6(a) and 6(b) show the reduced VDOS for samples with different cooling rates and sample sizes, respectively. Except the fluctuating structure induced by low-temperature relaxation, the VDOS is consistent with its zero-temperature counterpart obtained by the diagonalization method, evidenced by their similar frequencies of phonon bands. When the temperature induces thermal motion, the Debye level does not exist and the BP is ill-defined, as confirmed by a gap near zero frequency and multiple excess peaks around 3 THz.

For finite sample sizes, the absence of Debye level is observed in simulation[14,19] and experiment.[56] It is often claimed that BP is present at this situation, which may be due to the coarse-grain treatment that smears out the discrete phonon bands. However, caution must be taken because such smoothed BP may be highly dependent on the sample size, e.g., dependence should be obvious when we smooth the curves in Fig. 4(a). For real glasses with much lower cooling rates, stable structures bring about less localized modes, reducing greatly the coupling intensity between vibrational modes. Thus, the sample size for which BP are well-defined should be larger.

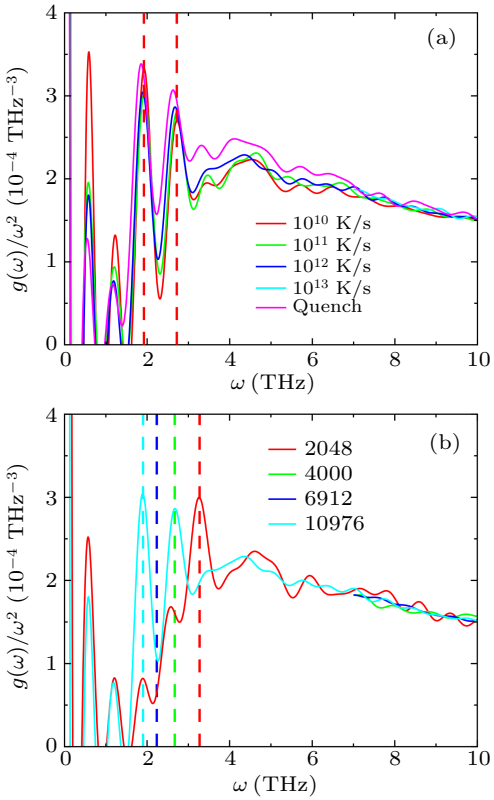


Fig. 6. Reduced VDOS obtained by the VACF method at 1 K for samples with different cooling rates (a) or sample sizes (b). The red vertical dashed lines in panel (a) represent the frequencies of the first and second phonon bands obtained by the diagonalization method as shown in Fig. 2. The vertical dashed lines in panel (b) represent the frequencies of the first phonon bands obtained by the diagonalization method as shown in Fig. 4.

4. Conclusions

To summarize, by molecular dynamics investigation of $Cu_{50}Zr_{50}$ metallic glasses, we clearly observed the resonant coupling of localized modes and phonon modes. Increasing cooling rate or sample size brings about the denser vibrational modes, resulting in the enhanced intensity of coupling effect. For samples of finite size, phonon modes do not fill up the low-frequency region and the coupling of phonon modes and localized modes is not sufficiently, giving rise to the ill-defined Debye level and BP. This situation remains valid at finite temperatures, even though anharmonicity comes into play.

In this paper, we mainly consider the vibration under harmonic regime. At a finite temperature that is not very low, such as room temperature, the anharmonic effect caused by thermal motion is significant and affects the shape of VDOS;

see Fig. 5(d). In such a situation, how localized modes and phonon modes couple to each other remains unknown. A method capable of extracting vibrational information at finite temperatures, based on the covariance matrix of particles' displacements,[57–60] provides a chance to investigate this problem.

Acknowledgements

Project supported by the National Outstanding Youth Science Fund Project (Grant No. 12125206), the Fund from the Basic Science Center for "Multiscale Problems in Nonlinear Mechanics" (Grant No. 11988102), and the General Project of the National Natural Science Foundation of China (Grant No. 11972345).

References

[1] Jiang M Q, Peterlechner M, Wang Y J, Wang W H, Jiang F, Dai L H and Wilde G 2017 *Appl. Phys. Lett.* **111** 261901
[2] Xu N, Vitelli V, Wyart M, Liu A J and Nagel S R 2009 *Phys. Rev. Lett.* **102** 038001
[3] Zeller R C and Pohl R O 1971 *Phys. Rev. B* **4** 2029
[4] Brink T, Koch L and Albe K 2016 *Phys. Rev. B* **94** 224203
[5] Liu H M, Lu C L, Wang K F, Liu J M, Wang Q and Dong C 2010 *Chin. Phys. B* **19** 017102
[6] Buchenau U, Nucker N and Dianoux A J 1984 *Phys. Rev. Lett.* **53** 2316
[7] Duval E, Saviot L, David L, Etienne S and Jal J F 2003 *Europhys. Lett.* **63** 778
[8] Zargar R, DeGiuli E and Bonn D 2016 *Europhys. Lett.* **116** 68004
[9] Zhang L, Zheng J, Wang Y, Zhang L, Jin Z, Hong L, Wang Y and Zhang J 2017 *Nat. Commun.* **8** 67
[10] Jezowski A, Strzhemechny M A, Krivchikov A I, Davydova N A, Szewczyk D, Stepanian S G, Buravtseva L M and Romantsova O O 2018 *Phys. Rev. B* **97** 201201
[11] Grigera T S, Martín-Mayor V, Parisi G and Verrocchio P 2003 *Nature* **422** 289
[12] Guerdane M and Teichler H 2008 *Phys. Rev. Lett.* **101** 065506
[13] Schirmacher W, Ruocco G and Scopigno T 2007 *Phys. Rev. Lett.* **98** 025501
[14] Shintani H and Tanaka H 2008 *Nat. Mater.* **7** 870
[15] Franz S, Parisi G, Urbani P and Zamponi F 2015 *Proc. Natl. Acad. Sci. USA* **112** 14539
[16] Chumakov A I, Monaco G, Monaco A, Crichton W A, Bosak A, Rueffer R, Meyer A, Kargl F, Comez L, Fioretto D, Giefers H, Roitsch S, Wortmann G, Manghnani M H, Hushur A, Williams Q, Balogh J, Parlinski K, Jochym P and Piekarz P 2011 *Phys. Rev. Lett.* **106** 225501
[17] Hu Y C and Tanaka H 2022 *Nat. Phys.* **18** 669
[18] Milkus R and Zaccone A 2016 *Phys. Rev. B* **93** 094204
[19] Yang J, Wang Y J, Ma E, Zaccone A, Dai L H and Jiang M Q 2019 *Phys. Rev. Lett.* **122** 015501
[20] Jakse N, Nassour A and Pasturel A 2012 *Phys. Rev. B* **85** 174201
[21] Ding J, Cheng Y Q, Sheng H, Asta M, Ritchie R O and Ma E 2016 *Nat. Commun.* **7** 13733
[22] Gurevich V L, Parshin D A and Schober H R 2003 *Phys. Rev. B* **67** 094203
[23] Caroli C and Lemaitre A 2020 *J. Chem. Phys.* **153** 144502
[24] Lerner E, During G and Bouchbinder E 2016 *Phys. Rev. Lett.* **117** 035501
[25] Schober H R and Laird B B 1991 *Phys. Rev. B* **44** 6746
[26] Ding J, Patinet S, Falk M L, Cheng Y and Ma E 2014 *Proc. Natl. Acad. Sci. USA* **111** 14052
[27] Argon A S 1979 *Acta Metall.* **27** 47
[28] Widmer-Cooper A, Perry H, Harrowell P and Reichman D R 2008 *Nat. Phys.* **4** 711
[29] Manning M L and Liu A J 2011 *Phys. Rev. Lett.* **107** 108302
[30] Yang J, Duan J, Wang Y J and Jiang M Q 2020 *Eur. Phys. J. E* **43** 56
[31] Duan J, Wang Y J, Dai L H and Jiang M Q 2023 *Phys. Rev. Mater.* **7** 013601
[32] Dong Y X, Zhang G H, Sun Q C, Zhao X D and Niu X N 2015 *Chin. Phys. Lett.* **32** 126201
[33] Bouchbinder E and Lerner E 2018 *New J. Phys.* **20** 073022
[34] Gelin S, Tanaka H and Lemaitre A 2016 *Nat. Mater.* **15** 1177
[35] Lerner E and Bouchbinder E 2023 *J. Chem. Phys.* **158** 194503
[36] Wang L, Ninarello A, Guan P, Berthier L, Szamel G and Flenner E 2019 *Nat. Commun.* **10** 26
[37] Mendelev M I, Kramer M J, Ott R T, Sordelet D J, Yagodin D and Popel P 2009 *Philos. Mag.* **89** 967
[38] Bell R J, Dean P and Hibbinsb.Dc 1970 *J. Phys. C* **3** 2111
[39] Xu N, Vitelli V, Liu A J and Nagel S R 2010 *Europhys. Lett.* **90** 56001
[40] Dickey J M and Paskin A 1969 *Phys. Rev.* **188** 1407
[41] Pan S P, Qin J Y, Wang W M and Gu T K 2011 *Phys. Rev. B* **84** 092201
[42] Shintani H and Tanaka H 2006 *Nat. Phys.* **2** 200
[43] Rainone C, Bouchbinder E and Lerner E 2020 *Proc. Natl. Acad. Sci. USA* **117** 5228
[44] Mizuno H, Shiba H and Ikeda A 2017 *Proc. Natl. Acad. Sci. USA* **114** E9767
[45] Beltukov Y M, Parshin D A, Giordano V M and Tanguy A 2018 *Phys. Rev. E* **98** 023005
[46] opu D, Stukowski A, Stoica M and Scudino S 2017 *Phys. Rev. Lett.* **119** 195503
[47] Taraskin S N and Elliott S R 1999 *Phys. Rev. B* **59** 8572
[48] Léonforte F, Tanguy A, Wittmer J P and Barrat J L 2006 *Phys. Rev. Lett.* **97** 055501
[49] Leonforte F, Boissiere R, Tanguy A, Wittmer J P and Barrat J L 2005 *Phys. Rev. B* **72** 224206
[50] Wuttke J, Petry W, Coddens G and Fujara F 1995 *Phys. Rev. E* **52** 4026
[51] Wischnewski A, Buchenau U, Dianoux A J, Kamitakahara W A and Zarestky J L 1998 *Phys. Rev. B* **57** 2663
[52] Charbonneau P, Kurchan J, Parisi G, Urbani P and Zamponi F 2014 *Nat. Commun.* **5** 3725
[53] Peng S X, Zhang C, Yang C, Li R, Zhang T, Liu L, Yu H B and Samwer K 2019 *J. Chem. Phys.* **150** 111104
[54] Ozawa M, Ikeda A, Miyazaki K and Kob W 2018 *Phys. Rev. Lett.* **121** 205501
[55] Ruta B, Baldi G, Giordano V M, Orsingher L, Rols S, Scarponi F and Monaco G 2010 *J. Chem. Phys.* **133** 041101
[56] Wang Y, Hong L, Wang Y, Schirmacher W and Zhang J 2018 *Phys. Rev. B* **98** 174207
[57] Das P, Ilyin V and Procaccia I 2019 *Phys. Rev. E* **100** 062103
[58] Ghosh A, Chikkadi V K, Schall P, Kurchan J and Bonn D 2010 *Phys. Rev. Lett.* **104** 248305
[59] Chen K, Manning M L, Yunker P J, Ellenbroek W G, Zhang Z, Liu A J and Yodh A G 2011 *Phys. Rev. Lett.* **107** 108301
[60] Wang X J, Duan J, Ding G, Lu Y Z, Lu X, Dai L H and Jiang M Q 2024 *Sci. China-Phys. Mech. Astron.* **67** 236112